npj computational materials

www.nature.com/npjcompumats

ARTICLE OPEN

Check for updates

Finding stable multi-component materials by combining cluster expansion and crystal structure predictions

Adam Carlsson[1]✉, Johanna Rosen[1] and Martin Dahlqvist[1]✉

A desired prerequisite when performing a quantum mechanical calculation is to have an initial idea of the atomic positions within an approximate crystal structure. The atomic positions combined should result in a system located in, or close to, an energy minimum. However, designing low-energy structures may be a challenging task when prior knowledge is scarce, specifically for large multi-component systems where the degrees of freedom are close to infinite. In this paper, we propose a method for identification of low-energy crystal structures within multi-component systems by combining cluster expansion and crystal structure predictions with density-functional theory calculations. Crystal structure prediction searches are applied to the Mo_2AlB_2 and Sc_2AlB_2 ternary systems to identify candidate structures, which are subsequently used to explore the quaternary (pseudo-binary) $(Mo_xSc_{1-x})_2AlB_2$ system through the cluster expansion formalism utilizing the ground-state search approach. Furthermore, we show that utilizing low-energy structures found within the cluster expansion ground-state search as seed structures within crystal structure predictions of $(Mo_xSc_{1-x})_2AlB_2$ can significantly reduce the computational demands. With this combined approach, we not only correctly identified the recently discovered $Mo_{4/3}Sc_{2/3}AlB_2$ *i*-MAB phase, comprised of in-plane chemical ordering of Mo and Sc and with Al in a Kagomé lattice, but also predict additional low-energy structures at various concentrations. This result demonstrates that combining crystal structure prediction with cluster expansion provides a path for identifying low-energy crystal structures in multi-component systems by employing the strengths from both frameworks.

npj Computational Materials (2023)9:21 ; https://doi.org/10.1038/s41524-023-00971-3

INTRODUCTION

Knowing the initial positions of atoms, or an approximate crystal structure prototype based on previous knowledge is preferred when performing a quantum mechanical calculation. This is commonly not much of a problem for systems with one or two elemental components, e.g., unary, and binary systems, since these have been investigated thoroughly. Villars and Iwata estimated that all unary systems and 72% of the potential binary systems have been experimentally studied. However, the potential elemental combinations increase rapidly for higher-order systems, which are also reflected in the number of materials systems reported as only 16% of ternary, 0.6% of quaternary, and 0.03% of quinary systems have been experimentally studied[1]. This demonstrates that experimental exploration of multi-component systems is still in its cradle and the avenues ahead are close to infinite. Theoretical studies may here serve as a complementary approach by predicting material combinations being most promising for future synthesis, as exemplified for ternary nitrides[2] and quaternary borides[3].

A certain group of materials that recently have attracted a large interest is atomically layered materials with interlayer interactions significantly stronger than van der Waals forces, hindering mechanical exfoliation. One such material group is MAX phases[4], which are comprised of transition-metal carbide and nitride (MX) layers interleaved by an A-group element. This structural arrangement along with the included elements often results in combined metallic and ceramic properties[5]. Furthermore, selective etching, also known as chemical exfoliation, of the A-element from the MAX phases has spurred an increased interest and has emerged as an alternative route for the preparation of a two-dimensional (2D) family of materials known as MXenes[6,7]. The search for additional multi-component materials with the possibility for exfoliation is thus of great interest, and the discovery of in-plane chemically ordered MAX phase quaternaries, coined *i*-MAX[8–10], has enabled the synthesis of MXenes with in-plane chemical or vacancy ordering, such as $Mo_{4/3}Y_{2/3}C$, $Mo_{4/3}C$, and $W_{4/3}C$, showing promise for energy storage and catalysis[9–12].

Similar to MAX phases are the layered metal boride-based materials, referred to as MAB phases, which consist of a transition metal (M), an A-group element (A), and boron (B). The mixing of metals in known ternary MAB phases have through theoretical guidance revealed both out-of-plane (*o*-MAB) and in-plane (*i*-MAB)[3,13] chemical ordering, where the latter phases have been converted into 2D derivatives coined boridene[14]. For the *o*-MAB phases, the chemical ordering of metal atoms was achieved by taking advantage of two distinctly different crystallographic sites and performing theoretical stability predictions, which revealed eleven stable *o*-MAB phases out of which Ti_4MoSiB_2, of a tetragonal *I*4/*mcm* symmetry, was later synthesized. The *i*-MAB phases $Mo_{4/3}Y_{2/3}AlB_2$ and $Mo_{4/3}Sc_{2/3}AlB_2$ (space group $R\bar{3}m$) were predicted thermodynamically stable by relaxing over 3,000 phases and were subsequently verified through powder synthesis[13]. The synthetized *i*-MAB phase $Mo_{4/3}Sc_{2/3}AlB_2$ with $R\bar{3}m$ symmetry will from this point forward be referred to as $Mo_{4/3}Sc_{2/3}AlB_2$, with fractional notations, whereas predicted phases of similar compositions will be referred to as $Mo_4Sc_2Al_3B_6$, with integer notations.

Different theoretical frameworks are utilized in the search for low-energy crystal structures. Examples of such are crystal structure prediction (CSP) frameworks[15–17] and cluster expansion (CE) methods[18]. CSP methods are independent of any a priori information of the crystal structure and typically employ evolutionary algorithms to explore the chemical phase space for low-

[1]Materials Design, Department of Physics, Chemistry, and Biology (IFM), Linköping University, SE-581 83 Linköping, Sweden. ✉email: adam.carlsson@liu.se; martin.dahlqvist@liu.se

energy basins and possibly stable candidate compounds[15–17]. For example, Rybkovskiy et al., studied the Mo-B system and predicted MoB_5 to be stable[19], and Xu et al., found a stable binary multi-layered MnB_2 phase with properties resembling a hard multi-functional material[20], both utilizing the CSP framework of USPEX[15–17]. Addition examples include CSP searches performed within the W-Cr-B ternary system where both W_4CrB_3 and W_2CrB_2 were found to be stable, which is in line with experimental findings, along with the yet to be synthesized $WCrB_2$, WCrB, and WCr_2B[21]. Wang et al. predicted and synthesized the first hexagonal MAB phase Ti_2InB_2 by employing USPEX algorithms[22]. The latter discovery increased the field of synthesizable layered MAB phases from orthorhombic and tetragonal to also include hexagonal symmetries[13]. However, the computational demands of CSP increase drastically with the increased complexity of the investigated system[23–25]. For example, Naumova et al. used CSP to search for structures in the quaternary C-H-N-O system, including pressure, which required approximately 1,800,000 density-functional theory (DFT) relaxations[26].

An alternative to the computationally demanding CSP is the use of methods such as CE which, in contrast to CSP, requires an a priori defined crystal structure. The expansion is carried out on one or multiple sublattices where parameterization is used to express the configurational dependence of physical properties such as energy[27], band gap[28,29], and magnetic interactions[30]. CE has also been used to explore the configurational space in layered hexagonal MAX phases upon mixing of metals in 41 quaternary systems[31] where the alloys were classified into three regimes—phase separation, weak ordering, and strong ordering. It was found that $(V_{2/3}Zr_{1/3})_2AlC$ should phase segregate into V_2AlC and Zr_2AlC[31]. This result, however, contradicts the experimental discovery of the in-plane ordered $(V_{2/3}Zr_{1/3})_2AlC$ *i*-MAX phase[8]. Note the structural differences between the MAX phase (which is the input for the CE model) and *i*-MAX phases, where the former has all atoms (V + Zr, Al, C) occupying hexagonal lattices while the latter combines honeycomb (for V), hexagonal (for Zr and C) and Kagomé-like (for Al) lattices. Furthermore, it has been demonstrated that the transformation from a hexagonal Al lattice to a Kagomé-like lattice gives rise to a significant decrease in energy for the material system[8,32]. This combined with an unsuccessfully truncated CE model due to a limited number of considered training structures may explain the discrepancy in why CE fails to predict the correct outcome in ref. [31]. Such inconsistency demonstrates the importance of using an appropriately truncated CE model when studying the mixing of metals in MAX phases[31,33–36].

In this work, we apply both CE and CSP methods to search for low-energy basins within the quaternary material system $(Mo_xSc_{1-x})_2AlB_2$ where $0 \le x \le 1$. Since we only vary the Mo to Sc ratio, while keeping Al and B fixed, the material system can be viewed as pseudo-binary. The reason for choosing Mo-Sc-Al-B as a model system is motivated by the recent discovery of *i*-MAB phase $Mo_{4/3}Sc_{2/3}AlB_2$, comprised of in-plane chemical ordering of Mo and Sc. An additional motivation is the structural resemblance with the ordered *i*-MAX phases[8] and discrepancies reported when investigating MAX phases with CE[31]. The question is if CE and/or CSP can be used to verify the synthesized $Mo_{4/3}Sc_{2/3}AlB_2$ ($R\bar{3}m$) compound discovered in ref. [13] while covering the phase space thoroughly with greater efficiency.

We herein demonstrate and discuss the possibilities and limitations of using CE and CSP independently when searching for low-energy structures and evaluating their thermodynamic stability. Despite CE being computationally efficient it is limited by its dependence on an a priori defined input structure, which limits the considered chemical phase space. CSP on the other hand does not require any structural input but demands significant computational resources. However, combining CE and CSP offers an efficient framework that yields reliable results when searching for low-energy basins as the drawbacks of each framework cancel out. The CSP is herein initially used to identify input structures for the CE models whereas the latter is used to explore the mixing and/or stability tendencies in $(Mo_xSc_{1-x})_2AlB_2$. Low-energy configurations found within the CE models are further used as seed structures within a final variational composition CSP search covering the complete phase space of $(Mo_xSc_{1-x})_2AlB_2$. Not only do we verify the stable and ordered *i*-MAB phase $Mo_{4/3}Sc_{2/3}AlB_2$ ($R\bar{3}m$), discovered in ref. [13], but also predict $Sc_4Mo_2Al_3B_6$ ($R3m$) as stable and nine additional $(Mo_xSc_{1-x})_2AlB_2$ structures as close to stable when the two frameworks are combined. We also identify two low-energy ternary MAB phase structures, Sc_2AlB_2 (*Pmmm*) and Mo_2AlB_2 (*P4/mbm*). Finally, the possibility of modifying the suggested framework for being applicable to any *n* dimensional material system with minor adjustments is discussed, i.e., by initiating a CSP search on the *n*–1 dimensionality subsystems followed by designing CE models on the obtained low-energy structures which results are then used to inspire a final CSP seach on the n dimensional material system.

RESULTS

Crystal structure prediction for ternary systems

Cluster expansion is an efficient approach for studying alloying in $(Mo_xSc_{1-x})_2AlB_2$ but requires an input structure to build a model upon. The hexagonal Ti_2InB_2 with $P\bar{6}m2$ symmetry and the orthorhombic Cr_2AlB_2, Mn_2AlB_2 and Fe_2AlB_2 with *Cmmm* symmetry[13,36] are examples of experimentally known MAB phases with M_2AB_2 composition. Note that these two prototype structures may not necessarily be of the lowest energy for Sc_2AlB_2 and Mo_2AlB_2 compositions and exploration for possible additional structures is thus motivated. We initiate the search for low-energy structures considering the Sc_2AlB_2 and Mo_2AlB_2 compositions by performing CSP searches. The corresponding evolution of the CSP search is shown in Fig. 1a, b where the formation enthalpy, using Eq. 2, is shown as a function of the number of generations. Identified low-energy structures are shown in Fig. 1c–f including the known $P\bar{6}m2$ and *Cmmm* symmetries.

The stability for Mo_2AlB_2, displayed in Fig. 1a, shows that the predicted lowest crystal structure after 72 generations is *P4/mbm* (illustrated in Fig. 1c) and it is close to stable with $\Delta H_{cp} = 5$ meV/atom. This structure is obtained after 42 generations and has previously been reported for W_2CrB_2 in ref. [21] with Mo/W and Al/Cr atoms in Wyckoff positions 4h and 2a, respectively, and originates from the V_3B_2 prototype structure. The structure found with the next-lowest energy is *Cmmm* (Fig. 1e), i.e., the Cr_2AlB_2 prototype structure, at $\Delta H_{cp} = 16$ meV/atom. Interesting to note is that the *Cmmm* structure have been reported as an intergrowth in the stable MoAlB structure of *Cmcm* symmetry[37]. Additionally, *Pmmm* (identified as the low-energy structure for Sc_2AlB_2 in Fig. 1b) and $P\bar{6}m2$ structures are found at $\Delta H_{cp} = 148$ and 89 meV/atom, respectively.

The evolution of the formation enthalpy for Sc_2AlB_2 is shown in Fig. 1b and illustrates two low-energy structures being close to stable with space group *Pmmm* (Fig. 1d) and *Cmmm* (Fig. 1e) at $\Delta H_{cp} = 22$ and 42 meV/atom, respectively. The *Pmmm* structure in Fig. 1d is comprised of an extra arrangement of Sc-Al and Sc-B layers constituting a layered B-Sc-B-Sc-Al-Sc-Al-Sc-Al-Sc-B-Sc-B stacking order. This is in contrast to the typical M_2AB_2 *Cmmm* structure, shown in Fig. 1e, with an Al-Sc-B-Sc-Al-Sc-B-Sc-Al stacking order. A noteworthy difference between the orthorhombic *Pmmm* and *Cmmm* and the hexagonal $P\bar{6}m2$ structures are the appearance of their B-layers, which have a zig-zag structure for the former while being planar for the latter. Additionally, the *P4/mbm* (identified as the low-energy structure for Mo_2AlB_2 in Fig. 1a and illustrated in Fig. 1c) and $P\bar{6}m2$ (Fig. 1f) structures are found at $\Delta H_{cp} = 139$ and 98 meV/atom, respectively. Detailed structural

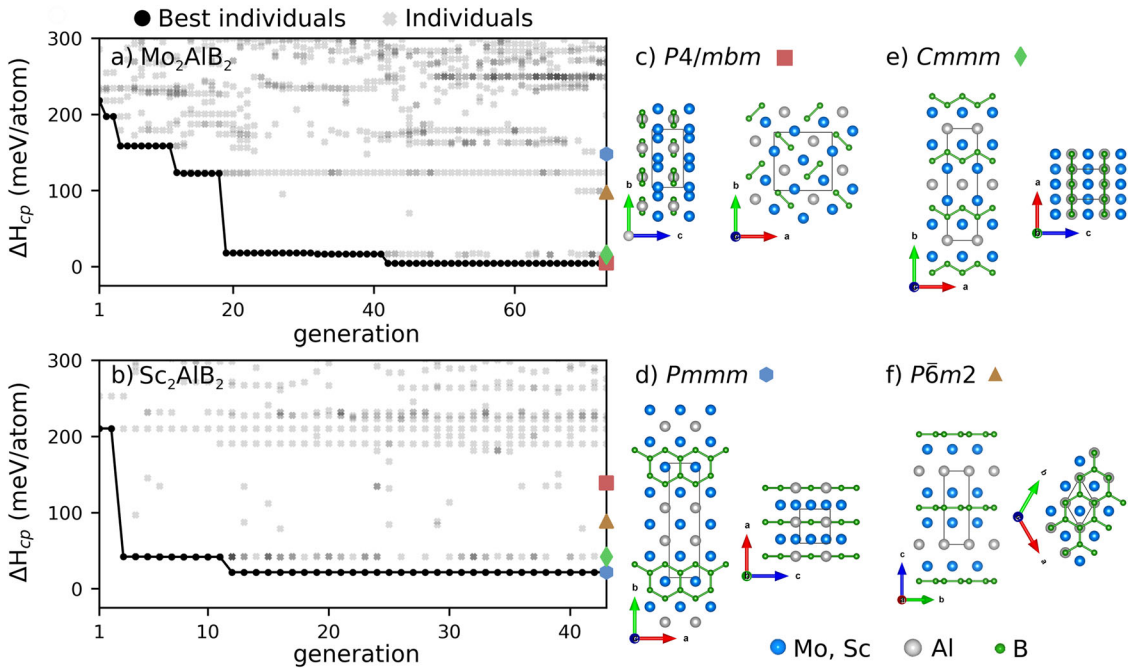

Fig. 1 The evolutionary trajectory of the formation enthalpy, ΔH_{cp}. The ΔH_{cp} of the ternary phases Mo_2AlB_2 (**a**) and Sc_2AlB_2 (**b**) along the evolutionary trajectory where lowest-energy structure in each generation is represented by a black circle and those at higher energies by gray crosses. Schematic illustration of predicted crystal structures of lowest energy corresponding to **c** Mo_2AlB_2 in space group *P4/mbm* and **d** Sc_2AlB_2 in space group *Pmmm*. Known M_2AB_2 prototype structures are illustrated with space group **e** *Cmmm* and **f** *Pō6m2*. Each structure is shown from two crystallographic different directions. Mo or Sc, Al, and B are represented by blue, gray, and green atoms.

information related to structures shown in Fig. 1c–f is found in Table 1.

Cluster expansion for identification of mixing tendencies

The four structures identified with low energy upon the CSP search in Fig. 1 (*Pmmm*, *P4/mbm*, *Cmmm*, and *Pō6m2*) are used as model structures in the search for low-energy structures within the pseudo-binary $(Mo_xSc_{1-x})_2AlB_2$ system. The Al and B sublattices are considered spectator atoms as the alloying is focused on mixing Mo and Sc on the metal lattice. The lattice constants used to construct the CE models for each considered symmetry were set to an average value of the relaxed Mo_2AlB_2 and Sc_2AlB_2 compositions. The CLEASE code offers three different methods for generating new configurations: (i) randomly, (ii) ground-state search, and (iii) probe structures. Within the ground-state search, the CE model aims at generating a new structure of low energy using a simulated annealing technique based on a pool of clusters from prior generations that are on or near the convex hull[38,39]. With this approach, the focus is on the exploration of low-energy regions within assigned compositional and structural boundaries. On the contrary, with the probe technique, structures are generated in order to increase the variance within the pool of configurations to consist of as independent structures as possible[40,41]. This approach may be utilized when exploring the complete chemical space of the system. Figure 1 illustrates the isostructural formation enthalpy ΔH_{iso} as a function of x in $(Mo_xSc_{1-x})_2AlB_2$ when using the three different generating strategies available in CLEASE and here applied to the *Pō6m2* system to show the similarities and differences between the techniques.

The outcome using randomly generated structures in Fig. 2a show less variation in ΔH_{iso} as compared to ground-state and probe generated structures in Fig. 2b, c. ΔH_{iso} for probe generated structures shows an increased variance but lacks in number of low-energy structures. The ground-state search gives the greatest number of low-energy structures, and this at a fairly low computational cost (~150 DFT calculations), but does not yield as many structures at higher energy as the probe does. Note that both probe and random mode will eventually find the same low-energy structures as the ground-state search but requires additional training configurations to be considered to improve the CE models.

Since we are interested in predicting low-energy structures, the results shown in Fig. 2 demonstrate the ground-state search technique to be most suitable, which motivates its use to pave the pathway towards the discovery of low-energy symmetries at a reduced computational effort rather than surveying the complete phase space with DFT calculations. All CE models considered herein are thus assembled using a iterative procedure with the ground-state search formalism. A database of different configurations of $(Mo_xSc_{1-x})_2AlB_2$ alloys are thus initially established for each considered CE model consisting of 25 randomly structures followed by at least 100 ground-state structures generated iteratively with each generation composed of 25–50 new generated configurations. Figure 3a–d shows the isostructural formation enthalpy ΔH_{iso} as a function of x in $(Mo_xSc_{1-x})_2AlB_2$ for the generated and relaxed ground-state configurations. We use ΔH_{iso} to illustrate possible mixing tendencies among the four model systems. In addition, the phase stability of each ground-state configuration within the CE models is shown in Fig. 2e–h by calculating the formation enthalpy ΔH_{cp}.

Neither *P4/mbm* (Fig. 3a) nor *Cmmm* (Fig. 3c) is found to have any strong preference for mixing Mo and Sc on the M-site, as indicated by the majority of structures with $\Delta H_{iso} > 0$. This is in contrast to *Pmmm* (Fig. 3b) and *Pō6m2* (Fig. 3d) which both show mixing tendencies as the majority of these structures have $\Delta H_{iso} < 0$. This is most pronounced for the hexagonal *Pō6m2* model system.

Corresponding stability for the four model systems, using Eq. 2, is displayed in Fig. 3e–h where the formation enthalpy ΔH_{cp} is shown as a function of x in $(Mo_xSc_{1-x})_2AlB_2$. Systems based on *P4/mbm* (Fig. 3e) and *Cmmm* (Fig. 3g) now show even fewer

Table 1. Space group, lattice parameters, Wyckoff position, and fractional atomic coordinates of predicted low-energy structures for Sc_2AlB_2 and Mo_2AlB_2.

Compound	Space group	ΔH_{cp} (meV/atom)	Lattice parameters (Å)	Atom (Wyckoff site)	Fractional coordinates		
					x	*y*	*z*
Sc_2AlB_2	*Pmmm*	22	$a = 3.20505$ Å	Sc1 (1a)	0.00000	0.00000	0.00000
			$b = 3.54197$ Å	Sc2 (2q)	0.00000	0.00000	0.27859
			$c = 11.96331$ Å	Sc3 (1d)	0.50000	0.00000	0.50000
				B1 (2r)	0.00000	0.50000	0.42464
				B2 (2t)	0.50000	0.50000	0.35200
				Al (2t)	0.50000	0.50000	0.14324
Sc_2AlB_2	*Cmmm*	42	$a = 11.81834$ Å	Al (2a)	0.00000	0.00000	0.00000
			$b = 3.18704$ Å	B (4 g)	0.21530	0.00000	0.00000
			$c = 3.59432$ Å	Sc (4h)	0.35903	0.00000	0.50000
Sc_2AlB_2	$P\bar{6}m2$	98	$a = 3.14487$ Å	Al (1a)	0.00000	0.00000	0.00000
			$c = 8.43732$ Å	B1 (1b)	0.00000	0.00000	0.50000
				B2 (1f)	0.66667	0.33333	0.50000
				Sc (2h)	0.33333	0.66667	0.29726
Sc_2AlB_2	*P4/mbm*	139	$a = 6.15293$ Å	Al (2b)	0.00000	0.00000	0.50000
			$c = 3.55744$ Å	B (4h)	0.59840	0.09840	0.50000
				Sc (4g)	0.17764	0.67764	0.00000
Mo_2AlB_2	*P4/mbm*	5	$a = 5.89216$ Å	Al (2b)	0.00000	0.00000	0.50000
			$c = 3.16159$ Å	B (4h)	0.61133	0.11133	0.50000
				Mo (4g)	0.17420	0.67420	0.00000
Mo_2AlB_2	*Cmmm*	16	$a = 11.63432$ Å	Al (2a)	0.00000	0.00000	0.00000
			$b = 3.08914$ Å	B (4g)	0.20781	0.00000	0.00000
			$c = 3.12544$ Å	Mo (4h)	0.35717	0.00000	0.50000
Mo_2AlB_2	$P\bar{6}m2$	89	$a = 3.04865$ Å	Al (1a)	0.00000	0.00000	0.00000
			$c = 7.35579$ Å	B1 (1b)	0.00000	0.00000	0.50000
				B2 (1f)	0.66667	0.33333	0.50000
				Mo (2h)	0.33333	0.66667	0.29350
Mo_2AlB_2	*Pmmm*	148	$a = 3.05299$ Å	Mo1 (1a)	0.00000	0.00000	0.00000
			$b = 3.18052$ Å	Mo2 (2q)	0.00000	0.00000	0.28063
			$c = 11.66041$ Å	Mo3 (1d)	0.50000	0.00000	0.50000
				B1 (2r)	0.00000	0.50000	0.42213
				B2 (2t)	0.50000	0.50000	0.34062
				Al (2t)	0.50000	0.50000	0.13401

tendencies for mixing Mo and Sc. For *Pmmm*, the Mo-rich region, which in Fig. 3b demonstrated mixing tendencies, is now found to be far from stable. For the $P\bar{6}m2$ symmetry in Fig. 3h, 6 structures are found stable in the region $0.5 \le x \le 0.67$.

To limit the number of structures chosen for further investigation, we introduce a cutoff at $\Delta H_{cp} < 10$ meV/atom. The CE models based on the *Pmmm* and *Cmmm* symmetries are thus sorted out as they all yield configurations at higher energies. A total of 15 structure fulfills $\Delta H_{cp} < 10$ meV/atom. One structure with the *P4/mbm* symmetry at $x = 1$ (also the input model structure identified in Fig. 1), with $\Delta H_{cp} = 5$ meV/atom, and 14 structures within the $P\bar{6}m2$ system. Additional structural information for the 15 structures is found in Supplementary Table 1. The three structures with the lowest ΔH_{cp} are illustrated in Fig. 4 from three different views.

Note that all structures in Fig. 4 bear the same layer sequence as the original $P\bar{6}m2$ symmetry in Fig. 1f but with a rearranged Al-layer (hexagonal lattice for the ternary M_2AlB_2 $P\bar{6}m2$). The structure at $x = 0.5$ symmetry (Fig. 4a), $\Delta H_{cp} = -12$ meV/atom, demonstrates an alternative stacking of in-plane ordered Mo-Mo-Sc-Sc interleaved by the Al-layer where Mo atoms are closer to the B layer while Sc atoms are closer to the Al-layer. The latter thus leads to a rearrangement of the Al-layer away from a hexagonal lattice. Similarly, the structure at $x = 0.56$ (Fig. 4b), $\Delta H_{cp} = -11$ meV/atom, does not display a particular order of Mo and Sc but noteworthy is that Sc is closer to the Al layer than Mo. The structure at $x = 0.67$ is predicted stable with $\Delta H_{cp} = -30$ meV/atom (Fig. 4c) and show clear in-plane order of Mo and Sc and where Al atoms form a Kagomé lattice (hexagonal lattice in $P\bar{6}m2$). The reason for the stable structure at $x = 0.67$ is further decomposed in Supplementary Fig. 1 where it is demonstrated that the major component for the decreased energy can be traced to the rearrangement of the Al atoms caused by the displacement of Sc towards the Al layer. Minor energy contributions are found from the Mo, B, and structural relaxations. Such secondary effects in spectator lattices are in agreement with similar observations demonstrated for the *i*-MAX phases reported in refs. [32,42] where it was demonstrated that metals (M′ and M″) with a significant size difference ($r_{M''} > r_{M'}$) in a ratio M′:M″ = 2:1 are mixed and ordered within the layered hexagonal MAX phase. This apparent in-plane order forces the larger M″ to be displaced towards the Al-layer. This procedure is illustrated in Supplementary Fig. 1 where the Al

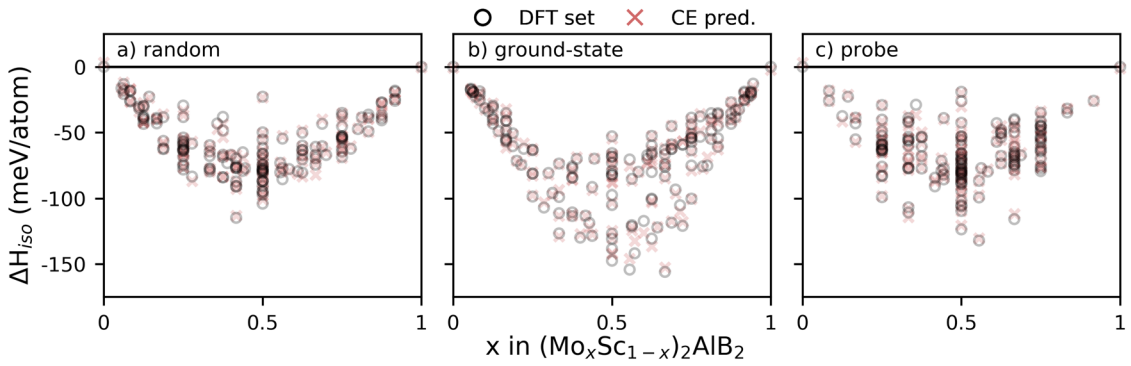

Fig. 2 The alternative techniques for generating configurations in CLEASE applied to the $P\bar{6}m2$ system. The training set is denoted by circles and predicted energies as crosses with at least 100 **a** randomly, **b** ground-state, and **c** probe generated structures.

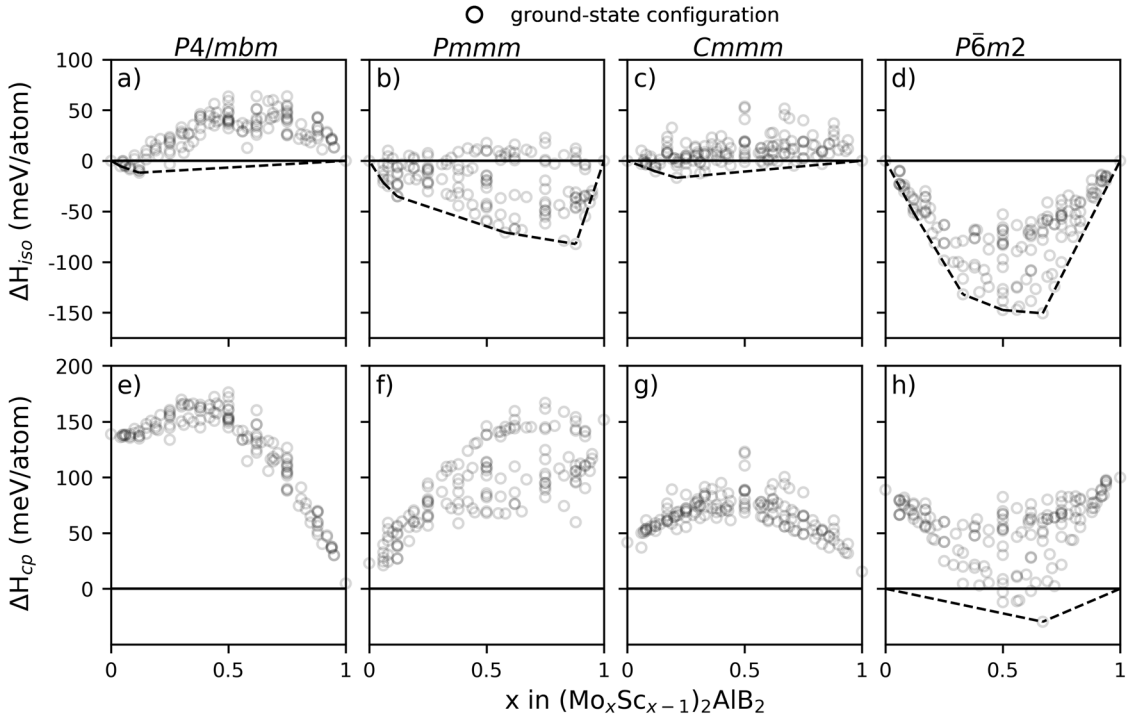

Fig. 3 Cluster expansion models applied to identify symmetries from the initial crystal structure prediction. a–**d** Isostructural formation enthalpy ΔH_{iso} and **e**, **f** formation enthalpy ΔH_{cp} of $(Mo_xSc_{1-x})_2AlB_2$ based on M_2AlB_2 in the (**a**, **e**) *P4/mbm*, (**b**, **f**) *Pmmm*, (**c**, **g**) *Cmmm*, and (**d**, **h**) $P\bar{6}m2$ crystal structure where M = Sc, Mo. CE generated structures are represented by gray circles.

lattice is observed to rearrange from a hexagonal lattice, which is the spectator lattice used within the CE model as defined by the input symmetry, to a Kagomé lattice when Sc is displaced towards the Al-layer.

The limitations of the cluster expansion formalism when used to pave the path towards stable and possibly synthesizable materials is the restriction defined by the input structure. Relying on an input structure may hinder the exploration of the phase space. Using CE alone is thus prone to miss valuable information hidden within the complete chemical space. An alternative approach that may circumvent this problem, and where the dependence of any initial structure is of lesser importance, or even neglected, is thus preferred.

Search for low-energy structures in a quaternary system

Next, we focus on exploring the chemical phase space within the $(Mo_xSc_{1-x})_2AlB_2$ system where $0 \le x \le 1$ through the use of the crystal structure prediction code USPEX. The aim is to identify stable low-energy structures and compare when no a priori information is used with seed structures retrieved from cluster expansion. Figure 5a illustrates the evolution of the CSP search for $x = 0.67$ where the formation enthalpy, using Eq. 2, is shown as a function of the number of generations without any seed structures (black) and with seed structures applied after 5 (red), 25 (blue), and 50 (yellow) generations. Included seed structures are gathered from the ground-state CE models depicted in Fig. 3.

Figure 5a illustrates the formation enthalpy, ΔH_{cp}, for $x = 0.67$ along the evolutionary trajectory. When no seeds are used, the predicted lowest-energy structure after 135 generations is an orthorhombic *Amm*2 structure with $\Delta H_{cp} = 29$ meV/atom. This structure is illustrated in Supplementary Fig. 2, with the corresponding structural information found in Supplementary Table 2, and bears resemblance with the orthorhombic *Cmmm* and *Pmmm* structures, illustrated in Fig. 1d, e, but with double-layers of Al and Mo. This is in contrast to the evolutionary searches using seed structures retrieved from the CE ground-state search in Fig. 3, which results in a predicted stable structure, $\Delta H_{cp} = -30$ meV/atom, with space group $R\bar{3}m$. This structure is

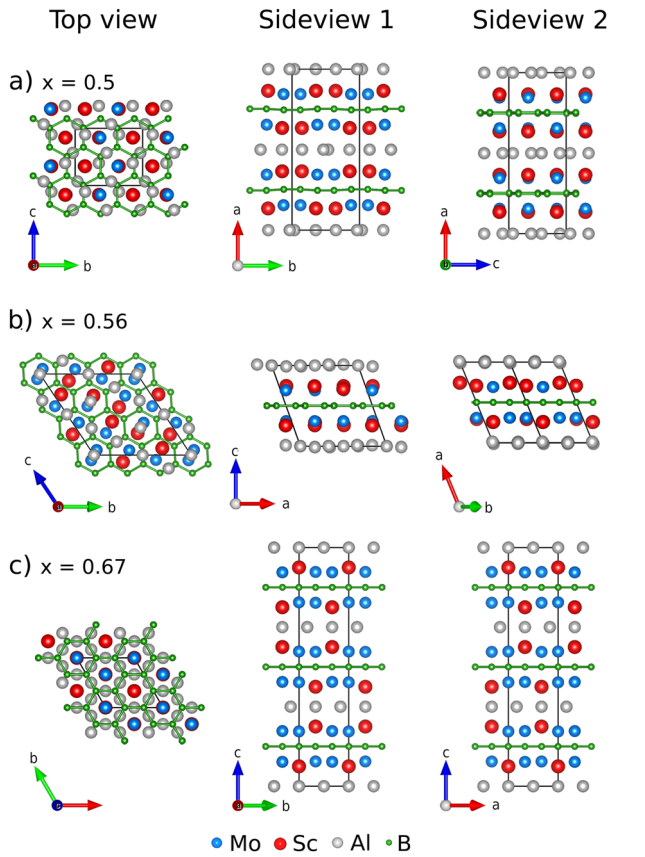

Fig. 4 Identified low-energy structures obtained from the CE models. The symmetries **a** $Cmc2_1$, **b** $P\bar{1}$, and **c** $R\bar{3}m$ illustrated from the top and two side views. The atomic species are denoted as the following: blue is Mo, red is Sc, gray is Al, and green is B.

found immediately after applying seeds following 5, 25, and 50 generations. Note that the number of individual structures generated with lower energy is observed to increase when seeds are applied at a later generation. This observation may conclude that using seeds not only predicts the global energy minima structure with greater efficiency but also significantly reduces the number of generations required to find additional low-energy basins.

The set of ground-state search generated structures with $\Delta H_{cp} < 10$ meV/atom in Fig. 3 are selected as seed structures for a variable composition search within the pseudo-binary $(Mo_xSc_{1-x})_2AlB_2$ system for $0 \le x \le 1$. Figure 5b shows the corresponding formation enthalpy ΔH_{cp} as a function of x limited to structures with $\Delta H_{cp} < 100$ meV/atom. Additional results including structures with $\Delta H_{cp} < 300$ meV/atom is shown in Supplementary Fig. 3. The predicted stable structures located on the convex hull are indicated by a filled blue circle and those above by red crosses. Two structures are found to be stable, $Mo_2Sc_4Al_3B_6$ ($R3m$) at $x = 0.33$ and $Mo_4Sc_2Al_3B_6$ ($R\bar{3}m$) at $x = 0.67$, with $\Delta H_{cp} = -18$ and -30 meV/atom, respectively. These structures are illustrated in Fig. 5c. Important to note is the discovery of the predicted stable $x = 0.33$ phase despite the lack of seed structures at that composition. Additional and similar structures above the convex hull but with $\Delta H_{cp} < 0$ are found at $x = 0.4, 0.5, 0.56, 0.57, 0.63$ and are referred to as metastable. A schematic illustration of the additional metastable low-energy structures is shown in Supplementary Fig. 2, and corresponding structural information can be found in Supplementary Table 2.

Common for the low-energy structures at $x = 0.33$ and 0.67 displayed in Fig. 5c are the flat Al-layers interleaved with M-B layers. The $Mo_4Sc_2Al_3B_6$ ($x = 0.67$) structure demonstrates more symmetric characteristics and higher order of Mo and Sc where Sc is located closer to the Al-layer while Mo is closer to the B-layer. $Mo_2Sc_4Al_3B_6$ ($x = 0.33$), on the other hand, yields less symmetric metal-layers, which is likely the reason for not being as stable $Mo_4Sc_2Al_3B_6$. Additional structural information for the stable $Mo_4Sc_2Al_3B_6$ and $Mo_2Sc_4Al_3B_6$ is found in Table 2.

Combining cluster expansion and crystal structure prediction

Using either cluster expansion (CE) or crystal structure prediction (CSP) alone when searching for low-energy structures in a multi-component system, like performed herein for the quaternary Mo-Sc-Al-B system, may yield limited and inadequate results. Even though CE is less computationally demanding out of the two approaches, it relies on a predefined input structure, which limits the considered chemical space when searching for low-energy basins. CSP searches, on the other hand, are independent of any initial structure but become more challenging when the dimensionality of the system is increased. The CSP searches applied to the ternary compositions consisted herein of an initial sampling of up to 200 DFT calculations followed by at least 50 generations, where each generation is comprised of 40 individual DFT calculations, before reaching desired convergence criteria. The CSP may occasionally yield a structure that is not the global energy minimum structure but rather a local minimum, as demonstrated in Fig. 5a. Users are thus promoted to be running several CSP searches on the same system in parallel to validate the stochastic results[43] which demands significant computational resources. Performing a variable composition search is arguably even more strenuous than considering a specific composition as the complexity of the system is increased. The variable composition search performed herein consists of 800 initially sampled structures followed by at least 50 generations each containing 100 new structures constructed by the variational operators.

The herein suggested solution for performing an efficient search in the quest for low-energy structures within a multi-component system is thus to combine CE and CSP. A proposed framework is illustrated in Fig. 6 for studying mixing and/or stability within higher order systems, such as the $(Mo_xSc_{1-x})_2AlB_2$ system considered in this work.

Before constructing the CE model systems for an n-dimensional system, a CSP search should be performed on the lower $n-1$ order systems constituting the system in focus, in our case the ternary systems Mo_2AlB_2 and Sc_2AlB_2, to identify possible low-energy structures to be used for constructing the CE models. These structures do not necessarily have to be stable, as exemplified herein for $P4/mbm$ Mo_2AlB_2 (5 meV/atom) and $Pmmm$ Sc_2AlB_2 (22 meV/atom). Additional low-energy symmetries, $P\bar{6}m2$ and $Cmmm$, found within the ternary CSP search are further considered. Note that the only CE model that resulted in strong mixing tendencies was the $P\bar{6}m2$ symmetry, which reflects the importance of considering alternative low-energy basin symmetries. Alternatively, additional low-energy symmetries may be obtained from literature, e.g., ref. $P\bar{6}m2$[22] and $Cmmm$ (Springer Materials: The Landolt-Börnstein database), which have previously been reported as M_2AB_2 structures. Next, CE models are constructed based on the pool of identified ternary low-energy symmetries from the CSP search. New structures are generated iteratively using the ground-state search technique for the exploration of low-energy basins within the studied chemical and structural-phase spaces. This analysis can be performed both in terms of isostructural enthalpy, ΔH_{iso}, and with respect to competing phases by calculating the formation enthalpy ΔH_{cp}. Configurations that are found close to stable, herein governed by the limit $\Delta H_{cp} < 10$ meV/atom, are selected as seed structures for a final variable compositional CSP search on the higher order material system.

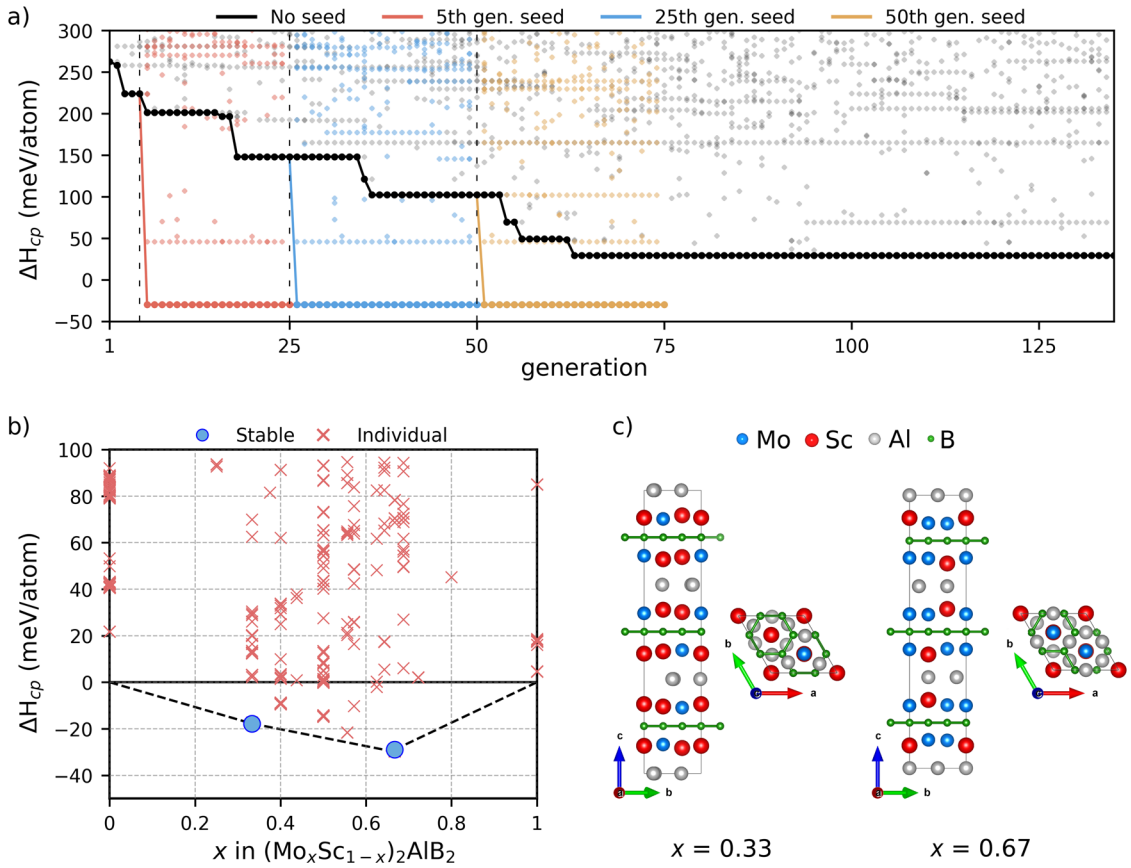

Fig. 5 Compositional crystal structure prediction including seeds from the cluster expansion models. a Formation enthalpy ΔH_{cp} of $(Mo_xSc_{1-x})_2AlB_2$, $x = 0.67$, along the evolutionary trajectory without (black) and with seed structures applied after 5 (red), 25 (blue), and 50 (yellow) generations. **b** ΔH_{cp} as a function of x in $(Mo_xSc_{1-x})_2AlB_2$ for predicted low-energy structures when performing the variational composition search. **c** Schematic illustration of the predicted stable structures located at $x = 0.33$ and $x = 0.67$ from two crystallographic directions.

Table 2. Space group, lattice parameters, Wyckoff position, and fractional atomic coordinates of predicted stable within the $(Mo_xSc_{1-x})_2AlB_2$, $0 \le x \le 1$, system.

x	Compound	Space group	ΔH_{cp} (meV/atom)	Lattice parameters (Å)	Atom (Wyckoff site)	Fractional coordinates		
						x	*y*	*z*
0.33	$Sc_4Mo_2Al_3B_6$	*R*3	−18	$a = 5.42213$ Å	Mo1 (3a)	0.00000	0.00000	0.56565
				$c = 23.28442$ Å	Mo2 (3a)	0.00000	0.00000	0.76901
					Sc1 (3a)	0.00000	0.00000	0.42328
					Sc2 (3a)	0.00000	0.00000	−0.09684
					Sc3 (3a)	0.00000	0.00000	0.09768
					Sc4 (3a)	0.00000	0.00000	0.24499
					Al (9b)	0.34849	0.18693	0.00066
					B1 (9b)	0.00214	0.66859	0.16730
					B2 (9b)	0.66665	0.66878	0.16729
0.67	$Mo_4Sc_2Al_3B_6$	$R\bar{3}m$	−30	$a = 5.37013$ Å	Mo1 (6c)	0.00000	0.00000	0.22946
				$c = 22.44751$ Å	Mo2 (6c)	0.00000	0.00000	0.43535
					Sc (6c)	0.00000	0.00000	0.08320
					Al (9e)	0.50000	0.00000	0.00000
					B (18g)	0.66519	0.00000	0.50000

DISCUSSION

Approaches like crystal structure prediction and cluster expansion are in general useful methods for predicting low-energy crystal structures. CE offers a robust and computationally effortless procedure where energies of generated crystal structures may be predicted by mapping the cluster interactions of a training set

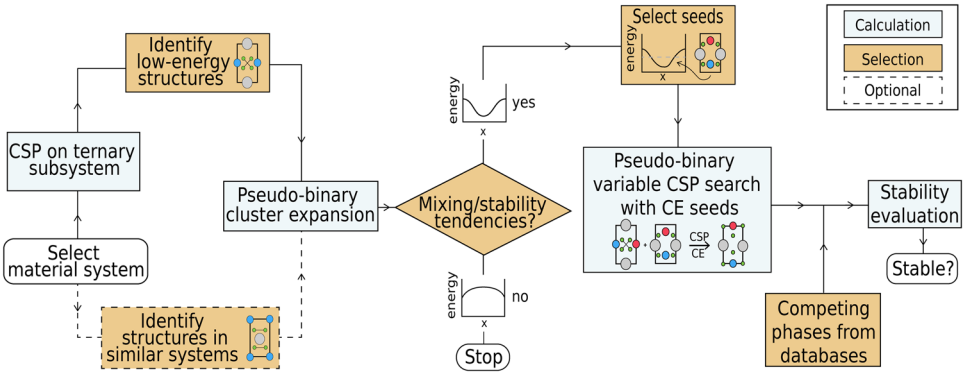

Fig. 6 Framework for combining cluster expansion with crystal structure prediction. Gray labels represent computational procedures, yellow labels denote sections that require manual input and optional modules are denoted by dashed lines.

onto a lattice of mixed atomic species. The model relies on a predefined lattice where mixing is to take place, which herein is performed on hexagonal, tetragonal, and orthorhombic symmetries of M_2AB_2 structures, and thus only explores a fraction of the complete energy landscape. Still, a CE model is herein shown to serve as a good seed generator for a CSP search. We find multiple crystal symmetries at various compositions in $(Mo_xSc_{1-x})_2AlB_2$, from orthorhombic and tetragonal symmetries at the ternary endpoints ($x = 0$ and 1) to trigonal, orthorhombic, and monoclinic symmetries in between by inspiring the CSP variational operators with the close to stable configurations found within the CE models.

Covering the complete chemical phase space of a quaternary system is a daunting task even though the crystal structure prediction algorithms utilized in USPEX provide a strong framework. Ref. [26] impressively performed a CSP search on the C-H-N-O material system while also considering pressure, which required the consideration of roughly 1,800,000 structural relaxations. Although we herein limit ourselves to consider the $(Mo_xSc_{1-x})_2AlB_2$ system, the structural variety is still extremely large. However, by combining CE with CSP, we show that the search for low-energy structures could be accelerated by utilizing the strengths of both frameworks.

We suggest that an iterative combination of the two methodologies, CE + CSP, could reduce the computational efforts while still thoroughly searching the energy landscape within higher order material systems for low-energy basins. The CE framework offers a computational effortless framework covering the initial grounds of the system, which may later be used as seed structures to further inspire the evolution of the CSP search. Multiple structures, including the *i*-MAB phase $Mo_{4/3}Sc_{2/3}AlB_2$ ($R\bar{3}m$) comprised of in-plane chemical ordering of Mo and Sc, are identified as stable or close to stable. This framework is applicable to any material system after only minor adjustments. The suggested approach is to initiate the search on the n–1 dimensionality systems, which constitutes the higher order, n-dimensional, system. Herein being the Mo_2AlB_2 and Sc_2AlB_2 systems. Once the foundation is established, the mixing and phase stability of the n dimensionality system ($(Mo_xSc_{1-x})_2AlB_2$) is motivated to be explored through variable compositional CSP searches with low-energy seed structures acquired from the CE models.

METHODS

Density-functional theory calculations

All structural relaxations required for the cluster expansion and crystal structure predictions were performed within the DFT framework, using the Perdew–Burke–Ernzerhof (PBE) generalized gradient approximation (GGA) to model the exchange correlation effects, and the all-electron projector augmented wave (PAW) method, as implemented in the Vienna Ab initio Simulation Package (VASP) version 5.4.1[44–47]. A plane wave energy cutoff set to 400 eV and a Monkhorst-Pack scheme used to sample the Brillouin zone with a k-point density of $2\pi \times 0.04$ Å^{-1} was selected. The chosen settings are motivated by the convergence tests performed in ref. [48], exploring quaternary metal borides, which yield energies accurate enough for efficient probing of the energy landscape. All structures were relaxed at ambient pressure and 0 K.

Evaluation of phase stability

The thermodynamical phase stability is herein determined by the formation enthalpy calculated at 0 K. The formation enthalpy of a general MAB phase $M_xA_yB_z$ is calculated by comparing the energy of $M_xA_yB_z$ with respect to all possible linear combinations of competing phases within the M-A-B material system. The pseudo-binary $(Mo_xSc_{1-x})_2AlB_2$ system considered herein is thus compared to all phases within the Mo-Sc-Al-B material system. The set of most competing phases constituting the minimum energy, which represents the decompositions within a quaternary Mo-Sc-Al-B system. The equilibrium simplex is obtained by solving

$$\min E_{cp}\left(b^{\mathrm{Mo}}, b^{\mathrm{Sc}}, b^{\mathrm{Al}}, b^{\mathrm{B}}\right) = \sum_{i}^{n} x_i E_i, \tag{1}$$

in which the left-handed side of Eq. (1) represents the equilibrium simplex energy for the given composition constraints b^{Mo}, b^{Sc}, b^{Al}, and b^{B} of elements Mo, Sc, Al, and B, respectively. The right-hand side denotes the set of linear combinations constructed of phase i with the amount x_i and energy E_i. The formation enthalpy ΔH_{cp} is thus calculated as

$$\Delta H_{cp}\left((Mo_xSc_{1-x})_2AlB_2\right) = E\left((Mo_xSc_{1-x})_2AlB_2\right) - \min E_{cp}\left(b^{\mathrm{Mo}}, b^{\mathrm{Sc}}, b^{Al}, b^{\mathrm{B}}\right), \tag{2}$$

where $E\left((Mo_xSc_{1-x})_2AlB_2\right)$ is the calculated energy of an arbitrary phase within $(Mo_xSc_{1-x})_2AlB_2$ and E_{cp} is the energy of the equilibrium simplex. Furthermore, a phase is attributed as stable when $\Delta H_{cp} < 0$ whereas a phase with $\Delta H_{cp} > 0$ is considered not stable or at best metastable. The set of competing phases considered herein are obtained from databases such as OQMD[49,50], Materials project[51], and Springer Materials (Springer Materials: The Landolt-Börnstein database). The complete set of competing phases is found in Supplementary Table 3 and the identified set of most competing phases for each considered composition is shown in Supplementary Table 4.

Cluster expansion

The energy of a crystalline solid within the cluster expansion[18] (CE) formalism is composed as a function of the underlying grid of

atomic sites or atomic arrangement of a given lattice. The herein used cluster expansion model is formulated using the cluster expansion in atomic simulation environment (CLEASE) code[52] motivated by its options to generate and predict new configurations. There are three techniques to generate configurations: randomly, through a ground-state search[38,39], and probe[40,41]. A brief introduction to the CE formalism is found in Supplementary Methods 1. The initial training set is composed of 25 randomly generated configurations. To improve the accuracy of the CE models and their predictability for exploration of low-energy regions a minimum of 100 configurations is generated iteratively through simulated annealing. The iterative procedure consists of generating a pool of 25–50 configurations within each generation. The evolution of the CE models upon the iterative procedure is shown in Supplementary Fig. 4. The randomly generated configurations for each CE model were constructed to consist of up to a maximum of 50 atoms and up to 100 atoms for configurations generated using the ground-state search.

Crystal structure prediction

All crystal structure prediction searches have employed the Universal Structure predictor: Evolutionary Xtallography (USPEX) code[17,53] where evolutionary algorithms are used to find a set of most optimal crystal structures within a given system. USPEX has been used for CSP searches within the ternary Mo_2AlB_2 and Sc_2AlB_2 systems and the quaternary (pseudo-binary) $(Mo_xSc_{1-x})_2AlB_2$ system. The ternary systems were initiated with 200 randomly generated structures whereas succeeding generations each contained 40 structures. The CSP search for $(Mo_xSc_{1-x})_2AlB_2$ was conducted by a variable composition search based on 800 randomly generated initial structures followed by succeeding generations containing 100 structures each. 60% of phases of the lowest energy in each generation were used as inspiration for the succeeding generation. 40% of each succeeding generation was generated by the heredity operator, 15% with lattice mutations, 15% with transmutation operations, 15% with soft-mode mutations, and 15% randomly. These settings apply to both CSP search scenarios, i.e., single, or variable composition.

DATA AVAILABILITY

The data supporting the results presented herein are available within the paper and the supplementary information. Relevant data is shared upon request.

CODE AVAILABILITY

The CLEASE and USPEX codes are available at https://gitlab.com/computationalmaterials/clease and https://uspex-team.org/en/uspex/downloads, respectively. All scripts used to obtain the formation enthalpies, analyze the data, and generate figures may be provided by the authors upon request.

Received: 19 May 2022; Accepted: 25 January 2023;
Published online: 08 February 2023

REFERENCES

1. Villars, P. & Iwata, S. Pauling file verifies/reveals 12 principles in materials science supporting four cornerstones given by Nature. *Chem. Met. Alloys* **6**, 81–108 (2013).
2. Sun, W. et al. A map of the inorganic ternary metal nitrides. *Nat. Mater.* **18**, 732–739 (2019).
3. Dahlqvist, M. et al. Out-of-plane ordered laminate borides and their 2D Ti-based derivative from chemical exfoliation. *Adv. Mater.* **33**, 2008361 (2021).
4. Sokol, M., Natu, V., Kota, S. & Barsoum, M. W. On the chemical diversity of the MAX phases. *Trends Chem.* **1**, 210–223 (2019).
5. Barsoum, M. W. The $M_{N+1}AX_N$ phases: a new class of solids: thermodynamically stable nanolaminates. *Prog. Solid State Chem.* **28**, 201–281 (2000).
6. Naguib, M. et al. Two-dimensional nanocrystals produced by exfoliation of Ti_3AlC_2. *Adv. Mater.* **23**, 4248–4253 (2011).
7. Vahid Mohammadi, A., Rosen, J. & Gogotsi, Y. The world of two-dimensional carbides and nitrides (MXenes). *Science* **372**, eabf1581 (2021).
8. Dahlqvist, M. et al. Prediction and synthesis of a family of atomic laminate phases with Kagomé-like and in-plane chemical ordering. *Sci. Adv.* **3**, e1700642 (2017).
9. Tao, Q. et al. Two-dimensional $Mo_{1.33}C$ MXene with divacancy ordering prepared from parent 3D laminate with in-plane chemical ordering. *Nat. Commun.* **8**, 14949 (2017).
10. Meshkian, R. et al. W-based atomic laminates and their 2D derivative W1.33 C MXene with vacancy ordering. *Adv. Mater.* **30**, e1706409 (2018).
11. Ahmed, B., Ghazaly, A. E. & Rosen, J. i-MXenes for energy storage and catalysis. *Adv. Funct. Mater.* **30**, https://doi.org/10.1002/adfm.202000894 (2020).
12. Persson, I. et al. Tailoring structure, composition, and energy storage properties of MXenes from selective etching of in-plane, chemically ordered MAX phases. *Small* **14**, e1703676 (2018).
13. Dahlqvist, M. et al. Theoretical prediction and synthesis of a family of atomic laminate metal borides with in-plane chemical ordering. *J. Am. Chem. Soc.* **142**, 18583–18591 (2020).
14. Zhou, J. et al. Boridene: two-dimensional $Mo_{4/3}B_{2-x}$ with ordered metal vacancies obtained by chemical exfoliation. *Science* **373**, 801–805 (2021).
15. Oganov, A. R. & Glass, C. W. Crystal structure prediction using ab initio evolutionary techniques: principles and applications. *J. Chem. Phys.* **124**, 244704 (2006).
16. Oganov, A. R., Lyakhov, A. O. & Valle, M. How evolutionary crystal structure prediction works—and why. *Acc. Chem. Res.* **44**, 227–237 (2011).
17. Lyakhov, A. O., Oganov, A. R., Stokes, H. T. & Zhu, Q. New developments in evolutionary structure prediction algorithm USPEX. *Comput. Phys. Commun.* **184**, 1172–1182 (2013).
18. Sanchez, J. M., Ducastelle, F. & Gratias, D. Generalized cluster description of multicomponent systems. *Phys. A: Stat. Mech. Appl.* **128**, 334–350 (1984).
19. Rybkovskiy, D. V., Kvashnin, A. G., Kvashnina, Y. A. & Oganov, A. R. Structure, stability, and mechanical properties of Boron-rich Mo–B phases: a computational study. *J. Phys. Chem. Lett.* **11**, 2393–2401 (2020).
20. Xu, C. et al. A first-principles investigation of a new hard multi-layered MnB_2 structure. *RSC Adv.* **7**, 10559–10563 (2017).
21. Hu, X. B. et al. Atomic-scale observation and analysis of chemical ordering in M_3B_2 and M_5B_3 borides. *Acta Mater.* **149**, 274–284 (2018).
22. Wang, J. et al. Discovery of hexagonal ternary phase Ti2InB2 and its evolution to layered boride TiB. *Nat. Commun.* **10**, 2284 (2019).
23. Song, Z. et al. First principles calculation on the newly superhard materials of W-B-C ternary system. *Solid State Commun.* **301**, 113705 (2019).
24. Kvashnin, A. G., Tantardini, C., Zakaryan, H. A., Kvashnina, Y. A. & Oganov, A. R. Computational search for new W–Mo–B compounds. *Chem. Mater.* **32**, 7028–7035 (2020).
25. Miao, N. et al. Computational prediction of boron-based MAX phases and MXene derivatives. *Chem. Mater.* **32**, 6947–6957 (2020).
26. Naumova, A. S., Lepeshkin, S. V., Bushlanov, P. V. & Oganov, A. R. Unusual chemistry of the C–H–N–O system under pressure and implications for giant planets. *J. Phys. Chem. A* **125**, 3936–3942 (2021).
27. van de Walle, A. A complete representation of structure–property relationships in crystals. *Nat. Mater.* **7**, 455–458 (2008).
28. Magri, R. & Zunger, A. Real-space description of semiconducting band gaps in substitutional systems. *Phys. Rev. B Condens. Matter* **44**, 8672–8684 (1991).
29. Ouyang, B. et al. Cluster expansion framework for the $Sr(Ti_{1-x}Fe_x)O_{3-x/2}$ $(0 < x < 1)$ mixed ionic electronic conductor: properties based on realistic configurations. *Chem. Mater.* **31**, 3144–3153 (2019).
30. Lavrentiev, M. Y., Dudarev, S. L. & Nguyen-Manh, D. Magnetic cluster expansion simulations of FeCr alloys. *J. Nucl. Mater.* **386–388**, 22–25 (2009).
31. Talapatra, A. et al. High-throughput combinatorial study of the effect of *M* site alloying on the solid solution behavior of M_2AlC MAX phases. *Phys. Rev. B* **94**, 104106 (2016).
32. Dahlqvist, M. & Rosen, J. The rise of MAX phase alloys—large-scale theoretical screening for the prediction of chemical order and disorder. *Nanoscale* **14**, 10958–10971 (2022).
33. Arróyave, R. & Radovic, M. Ab initio investigation of $Ti_2Al(C,N)$ solid solutions. *Phys. Rev. B* **84**, 134112 (2011).
34. Arróyave, R. et al. Does aluminum play well with others? Intrinsic Al-A alloying behavior in 211/312 MAX phases. *Mater. Res. Lett.* **5**, 170–178 (2017).
35. Arróyave, R., Talapatra, A., Duong, T., Son, W. & Radovic, M. Out-of-plane ordering in quaternary MAX alloys: an alloy theoretic perspective. *Mater. Res. Lett.* **6**, 1–12 (2018).
36. Wong, Z. M. et al. High performance photocatalytic and thermoelectric two-dimensional asymmetrically ordered Janus-like MXene alloys. *Mater. Adv.* **1**, 1176–1185 (2020).

37. Kota, S. et al. Synthesis and characterization of an alumina forming nanolaminated boride: MoAlB. *Sci. Rep.* **6**, 26475 (2016).
38. van de Walle, A. & Ceder, G. Automating first-principles phase diagram calculations. *J. Phase Equilibria* **23**, 348 (2002).
39. Urban, A., Seo, D.-H. & Ceder, G. Computational understanding of Li-ion batteries. *NPJ Comput. Mater.* **2**, 16002 (2016).
40. Seko, A. & Tanaka, I. Cluster expansion of multicomponent ionic systems with controlled accuracy: importance of long-range interactions in heterovalent ionic systems. *J. Phys.Condens. Matter* **26**, 115403 (2014).
41. Seko, A., Koyama, Y. & Tanaka, I. Cluster expansion method for multicomponent systems based on optimal selection of structures for density-functional theory calculations. *Phys. Rev. B* **80**, 165122 (2009).
42. Dahlqvist, M., Petruhins, A., Lu, J., Hultman, L. & Rosen, J. Origin of chemically ordered atomic laminates (i-MAX): expanding the elemental space by a theoretical/experimental approach. *ACS Nano* **12**, 7761–7770 (2018).
43. Liu, X., Niu, H. & Oganov, A. R. COPEX: co-evolutionary crystal structure prediction algorithm for complex systems. *NPJ Comput. Mater.* **7**, 199 (2021).
44. Perdew, J. P., Burke, K. & Ernzerhof, M. Generalized gradient approximation made simple. *Phys. Rev. Lett.* **77**, 3865–3868 (1996).
45. Blöchl, P. E. Projector augmented-wave method. *Phys. Rev. B* **50**, 17953–17979 (1994).
46. Kresse, G. & Hafner, J. Ab initio molecular dynamics for liquid metals. *Phys. Rev. B* **47**, 558–561 (1993).
47. Kresse, G. & Furthmüller, J. Efficiency of ab-initio total energy calculations for metals and semiconductors using a plane-wave basis set. *Comput. Mater. Sci.* **6**, 15–50 (1996).
48. Dahlqvist, M. & Rosen, J. Chemical order or disorder—a theoretical stability expose for expanding the compositional space of quaternary metal borides. *Mater. Adv.* **3**, 2908-2917 (2022).
49. Kirklin, S. The Open Quantum Materials Database (OQMD): assessing the accuracy of DFT formation energies. *NPJ Comput. Mater.* **1**, 15010 (2015).
50. Saal, J. E. Materials design and discovery with high-throughput density functional theory: The Open Quantum Materials Database (OQMD). *JOM* **65**, 1501–1509 (2013).
51. Jain, A. et al. The materials project: a materials genome approach to accelerating materials innovation. *APL Mater.* **1**, 011002 (2013).
52. Chang, J. H. et al. CLEASE: a versatile and user-friendly implementation of cluster expansion method. *J. Phys. Condens. Matter* **31**, 325901 (2019).
53. Glass, C. W., Oganov, A. R. & Hansen, N. USPEX—evolutionary crystal structure prediction. *Comput. Phys. Commun.* **175**, 713–720 (2006).

ACKNOWLEDGEMENTS

M.D. acknowledges support from the Swedish Research council through project 2019-05047. J.R. acknowledges funding from the Knut and Alice Wallenberg (KAW) Foundation for a Fellowship/Scholar Grant and Project funding (KAW 2020.0033). The calculations were conducted using supercomputer resources provided by the Swedish National Infrastructure for Computing (SNIC) at the National Supercomputer Center (NSC) and the High Performance Computing Center North (HPC2N), partially founded by the Swedish Research Council through grant agreement no. 2018-05973.

AUTHOR CONTRIBUTIONS

A.C. and M.D. conceived the project, which was supervised by M.D. and J.R. A.C. performed all data analysis, calculations, and drafted the manuscript. All Authors reviewed and edited the manuscript.

FUNDING

Open access funding provided by Linköping University.

COMPETING INTERESTS

The authors declare no competing interests.

ADDITIONAL INFORMATION

Supplementary information The online version contains supplementary material available at https://doi.org/10.1038/s41524-023-00971-3.

Correspondence and requests for materials should be addressed to Adam Carlsson or Martin Dahlqvist.